Biochimica et Biophysica Acta 1828 (2013) 499–509

Contents lists available at SciVerse ScienceDirect

Biochimica et Biophysica Acta

journal homepage: www.elsevier.com/locate/bbamem

Modeling of non-covalent complexes of the cell-penetrating peptide CADY and its siRNA cargo

Jean-Marc Crowet [a,*], Laurence Lins [a], Sébastien Deshayes [b], Gilles Divita [b], May Morris [b], Robert Brasseur [a], Annick Thomas [c]

[a] Centre de Biophysique Moléculaire Numérique, Gembloux Agro-Bio Tech, University of Liège, Gembloux, Belgium
[b] Centre de Recherches de Biochimie Macromoléculaire, CRBM-CNRS, UMR-5237, UM1-UM2, Department of Molecular Biophysics and Therapeutics, University of Montpellier, Montpellier, France
[c] Institut de Pharmacologie et de Biologie Structurale, IPBS-CNRS, UMR-5089, University of Toulouse III, Toulouse, France

ARTICLE INFO

Article history:
Received 4 April 2012
Received in revised form 9 August 2012
Accepted 7 September 2012
Available online 19 September 2012

Keywords:
Cell penetrating peptide
siRNA
CADY
Non-covalent complex
Molecular modeling
Molecular dynamics

ABSTRACT

CADY is a cell-penetrating peptide spontaneously making non-covalent complexes with Short interfering RNAs (siRNAs) in water. Neither the structure of CADY nor that of the complexes is resolved. We have calculated and analyzed 3D models of CADY and of the non-covalent CADY–siRNA complexes in order to understand their formation and stabilization. Data from the ab initio calculations and molecular dynamics support that, in agreement with the experimental data, CADY is a polymorphic peptide partly helical. Taking into consideration the polymorphism of CADY, we calculated and compared several complexes with peptide/siRNA ratios of up to 40. Four complexes were run by using molecular dynamics. The initial binding of CADYs is essentially due to the electrostatic interactions of the arginines with siRNA phosphates. Due to a repetitive arginine motif (XLWR(K)) in CADY and to the numerous phosphate moieties in the siRNA, CADYs can adopt multiple positions at the siRNA surface leading to numerous possibilities of complexes. Nevertheless, several complex properties are common: an average of 14 ± 1 CADYs is required to saturate a siRNA as compared to the 12 ± 2 CADYs experimentally described. The 40 CADYs/siRNA that is the optimal ratio for vector stability always corresponds to two layers of CADYs per siRNA. When siRNA is covered by the first layer of CADYs, the peptides still bind despite the electrostatic repulsion. The peptide cage is stabilized by hydrophobic CADY–CADY contacts thanks to CADY polymorphism. The analysis demonstrates that the hydrophobicity, the presence of several positive charges and the disorder of CADY are mandatory to make stable the CADY–siRNA complexes.

1. Introduction

The therapeutic application of molecules such as peptides, proteins, drugs and nucleic acids is directly related to their plasma membrane permeability and to their capacity to reach biological targets within cells [1]. siRNAs specifically control protein activation and/or gene expression post-transcriptionally and have thus important therapeutic potentialities. They are of a major interest for future therapies in several diseases, including cancer [2,3] and the main obstacle to their clinical applications, as in most nucleic acid-based strategies, remains their poor cellular uptake and bioavailability [4,5]. Among the different carriers that were developed to facilitate membrane translocation of therapeutic molecules (liposomes, biopolymers, retroviruses, …), Cell Penetrating Peptides (CPPs) are very promising [6,7]. CPPs are highly-charged and relatively short (less than 30 residues). Two classes of CPP–cargo complexes have been described resulting in either a covalent link between the CPP and its cargo, or the non-covalent interactions of several CPPs with a cargo [7,8]. The latter offers the advantage to simplify the protocol of conjugation since there is no need for a chemical linkage; it also reduces the likelihood of CPP interference with the biological activity of the therapeutic molecule since therapeutic effects likely require the free form of the cargo [1]. Recently, the non-covalent strategy based on MPG/CADY amphipathic peptides has been successfully applied for both in cellulo and in vivo siRNA delivery [9,10] and was extended to CPPs originally used to make conjugates [11,12].

The non-covalent CPPs, CADY, MPG and PEP-1, associate rapidly with their cargo by combining both electrostatic and hydrophobic interactions to form stable complexes [7,10,13–17]. For MPG and PEP1, optimal biological responses are observed for a peptide–cargo molar ratio between 10/1 and 25/1 [9,14,18,19]. CD and FTIR experiments have demonstrated that CADY is mainly random coil in water and more α-helical in the presence of its siRNA cargo [14] while Pep-1 and MPG are random coil in water at low concentrations and remain so in the presence of their cargo [15]. CADY is monomeric in solution and possesses a cysteamide residue on its C-terminal end like MPG. This residue was originally added to enable the attachment

* Corresponding author.
E-mail address: jmcrowet@ulg.ac.be (J.-M. Crowet).

0005-2736/$ – see front matter © 2012 Elsevier B.V. All rights reserved.
http://dx.doi.org/10.1016/j.bbamem.2012.09.006

of probes and drugs but was shown to lead to more efficient cellular uptakes [20].

Cellular uptakes of the CPP–cargo complexes were long thought to be independent of endocytosis, requiring no energy. However, Richard et al. highlighted the artifacts in earlier studies and proposed a mechanism associated with the endosomal pathway [21]. Nowadays, although the cellular uptake mechanism of most covalent cargo–CPP complexes is believed to involve endosomal routes, the mechanisms remain unclear for the non-covalent cargo–CPP complexes [15,22,23]. Numerous studies have shown that the cell permeability of these non-covalent CPP–cargo complexes does not necessarily involve the endosomal pathway and that they can enter cells by different ways including a direct uptake which depends on their nature and local concentration [15,24].

The permeability problem could be different for free CPPs. Mechanisms of direct translocation have been proposed such as the "carpet model" [25], transient pore formation [26] or reverse micelle formation [27]. Recently, molecular dynamics studies of the interactions of Penetratin, TP10, TAT and poly-arginine peptides with lipid bilayer have been described [28–30]. Herce et al. carried out all-atom simulations of the HIV-1 TAT peptide in the presence of a membrane and proposed a mechanism of translocation in four steps including the formation of a transient water pore and the diffusion of peptides at the pore surface to cross the membrane [28,31]. An alternative mechanism was proposed by Yesylevskyy et al. in which Penetratin and TAT peptides enter cells by macropinocytosis. The peptides induce a membrane curvature ultimately leading to the encapsulation of a peptide cluster [29].

The structure of the non-covalent CPP–cargo complexes has been studied by dynamic light scattering and electron microscopy and nanoparticles with sizes between 70 and 200 nm were observed [14,15,18,23]. Gaining further information on the structures of the non-covalent complexes should be valuable in the understanding of their complex formation and their translocation through the membranes.

The present work focuses on the secondary amphipathic CADY-peptide and on its capacity to spontaneously form non-covalent complexes with siRNA in water. These complexes promote the nucleic acid internalization and a biological response in cellulo [10]. We start by calculating the 3D models of CADY because no experimental model has been resolved. In 2006, we developed PepLook, a Boltzmann stochastic algorithm, to calculate the structure of peptides from sequences [32]. The conformation of CADY was reported to vary with the media [14] and structural polymorphism was demonstrated to be important for the activity and permeability of some CPPs [33,34]. Special attention is paid to polymorphism in PepLook since, besides the best 3D model named the Prime that was shown to be comparable to NMR models [32], the population of low energy models is also sorted enabling to evaluate the peptide structural polymorphism.

When disordered peptides build up complexes, their initial diversity of structures may lead to different solutions of binding or, the binding step can select one conformation. To take the problem into account we calculated several CADY–siRNA complexes from different models of CADY and compared them. To calculate complexes, we used a screening docking procedure. In 1986, Brasseur et al. developed Hypermatrix to analyze the interaction of peptides with lipids [35–38] and was recently used to compare the mechanism of interaction of the derived-CRAC motifs with cholesterol [39,40]. Efficient CRAC motifs were shown to pinch the polar OH head of cholesterol, saturating its H-donor and H-acceptor capacities and impairing its polar interactions with phosphatidylcholine. In the present work, the initial Hypermatrix procedure in the membrane was modified to dock molecules in the 3 dimensions of a homogenous medium as water. Last, several complexes were relaxed by all-atom molecular dynamics using GROMACS [41]. Cargo–CPP complexes were analyzed and compared to predict the main rules of their formation and stability.

2. Material and methods

2.1. Peptide and siRNA models

CADY is a 20 residue peptide (Table 1) with its N and C-ends blocked by an acetyl and a cysteamide moiety, respectively. We used two siRNAs (Table 1). The first one is the PDB model from 2ZI0 and will be named siRNA1. The second corresponds to the anticyclin B1 siRNA (siRNA2) and it was calculated using Coot in a double helix A [42]. siRNA2 possesses two flipping thymines at both ends.

Different 3D models of CADY have been calculated. First, an α-helix was constructed and minimized by conjugate gradient using HyperChem 5.0 (Hypercube Inc.). Then, two models were calculated with PepLook [32]. Briefly, the 3D models are built from the sequence by introducing backbone angle values randomly drawn from a set of 64 couples of phi/psi angles derived from a database of protein PDB models. At each step, $2 \cdot 10^5$ different models are calculated and their energy is used for ranking. Backbone angle values that give either good or bad solutions are identified. The relative probability of picking up one of the 64 phi/psi values for a residue is then modulated according to its chances of inducing good or bad conformations in the previous steps. Calculations are automatically stopped when the pattern of probability of the phi-psi angles remains constant for at least five steps. The best model is the Prime and the 50 models of lower energy are sorted to characterize the peptide polymorphism.

Models are all-atoms and their energies are computed as described in Thomas et al. [32] taking into account all interactions between non-bound atoms with a cut off of 2 nm. Energy terms are Van der Waals (Lennard-Jones), electrostatic (coulomb with an exponentially variable dielectric constant from 1 to 80) and two hydrophobicity terms, one for intra and intermolecular atom interactions and the second for solvent effect. The first terms use atom transfer energy (Etr) and atom distances, the second one uses atom accessible surface area and atom Etr in the corresponding solvent, as previously described [32,43].

The two PepLook models used in the study were the Prime models calculated in two different external media: a homogenous water solvent and a water/charged lipid plane interface (50% DOPC:50% DOPG). For complex formation, the model of CADY predicted at a charged interface was used as the best starting structure for the complex computation regarding the peptide conformation. For the interface conditions, at each PepLook step, all models are tested for 1000 orientations at 9 positions i.e. every Å of a 9 Å thick slab interface [44]. The minimal energy restraint value of insertion in the interface is added to the model energy value to rank the models.

2.2. CADY–siRNA complexes

The procedure for calculating the siRNA–CADY complexes is modified from the Hypermatrix 2D procedure in membranes [35–37] to dock molecules in 3 dimensions. An immobile molecule is the target and a partner initially set at 360 different positions equally spaced around the target mass center is moved (translations and rotations) around. The energy of partner interactions is calculated at each position. The immobile target was one of the 3D models of siRNAs, and moving partners were the 3D models of CADY. We used three models of CADY; the PepLook Primes of CADY calculated in water and in the interface and, the α helix model of CADY.

Table 1
CADY and siRNA sequences.

Molecule	Sequence
CADY	Ac-GLWRALWRLLRSLWRLLWKA-cysteamide
19 bp siRNA (2ZI0) (siRNA1)	5′ AGACAGCAUUAUGCUGUCU 3′ (sense strand)
siRNA anti-cyclin B1 (siRNA2)	5′ GAAAUGUACCCUCCAGAAATT 3′ (sense strand)

CADYs are moved away from the siRNA mass center by steps of 1 Å up to 80–100 Å. At each step, 90 rotations of CADY are made with a maximal magnitude of 360°. The energies of partner interactions are calculated. The energy and relative positions of all complexes are stored and complexes are calculated by the sequential addition of CADYs to form low-energy systems.

2.3. Molecular dynamics

For molecular dynamics computations, we used the GROMACS and the AMBER 99 force fields [45] to which we had to add a description of the cysteamide residue (CYA) derived from the cysteine residue. Molecular dynamics were performed for the interfacial Prime model of PepLook and the helix model of CADY and for the four Hypermatrix complexes made with siRNA2 as detailed in Table 2. All systems were solvated with TIP3P water and neutralized with Na^+ or Cl^-. The size of the triclinic boxes was defined to let at least 1 nm between the solute and the box. All systems were first minimized by 2000 steps of the steepest descent and then run for 50 ps of simulation with the peptides and the siRNA under position restraints in periodic boundary conditions (PBC) using a 2 fs time step. Dynamics were carried out in NPT conditions (310 K and 1 bar). Temperature and pressure were maintained using the bath method of Berendsen [41]. Electrostatic interactions were treated using the particle mesh Ewald (PME) method [46], and Van der Waals interactions were treated with the shift method. All cutoffs were set to 1.4 nm. Bonds were maintained with the SHAKE algorithm [47]. Positions and velocities of atoms in the system were saved every 10 ps. All computations, corresponding to a total time of 465 ns, were performed on three computers with Intel bi-Xeon quad core (2.33 GHz). The trajectories were performed and analyzed with GROMACS 3.3.3 tools. The results of the first runs are described and differences observed in the repeats, if any, are specified in the text.

2.4. MHP (molecular hydrophobicity potential)

MHP is a three-dimensional plot of the hydrophobicity isopotential surface of a molecule or of a group of molecules. The plot is created to visualize the system amphipathy as described by Brasseur in 1991 [48] and is calculated by summing the contribution of all atoms. Hydrophobicity at a point of space is derived from atom Etr and decreases exponentially with the distance between the surface of the atom and this point [48]. In the MHP plots, surfaces joining all points of ± 0.418 kJ are drawn, green for the hydrophilic potential, brown for the hydrophobic potential.

Table 2
List of molecular dynamic simulations.

Simulation name	System composition	Box size (nm^3)	Number of simulations	Simulation times (ns)
H1-3	CADY (α helix)/$water_{3168}$/Cl_{-5}	5×5×4	3	50
P1-3	CADY (interfacial PepLook)/$water_{3811}$/Cl_{-5}	4×6×5	3	50
CH1	siRNA2/CADY (α $helix)_{13}$/$water_{23062}$/Cl_{-25}	12×8×8	1	50
CH2	siRNA2/CADY (α $helix)_{38}$/$water_{46539}$/Cl_{-150}	13×11×11	1	20
CP1	siRNA2/CADY $(PepLook)_{14}$/$water_{26258}$/Cl_{-30}	12×9×8	1	50
CP2	siRNA2/CADY $(PepLook)_{36}$/$water_{42784}$/Cl_{-140}	12×11×11	1	20

2.5. Properties of molecules and complexes

All molecules and complexes were analyzed using Pex [49] to detect residues in interaction, to calculate accessible and contact surfaces (hydrophobic and hydrophilic), lengths and volumes of complexes, and the energy of residues in interaction. Accessible Surface Area (ASA) was calculated using the method of Shrake and Rupley (162 dots) and a water molecule radius of 1.4 Å as previously reported [50,51]. To characterize peptide−siRNA and peptide−peptide interactions, atomic contacts were counted by using a distance cut off between atom centers of 0.35 nm. A single contact, the shortest, was accepted per pair of residues of different chains. Contacts were classified according to the type of amino acid, to their mapping in nucleotides (phosphate, sugar, base) and in amino acids (backbone, side chains) and to their types (salt bridges, hydrogen bonds, hydrophobic contacts and Van der Waals). These types were defined as in Lejeune et al. in 2005 [52]. The interactions are salt bridges when nucleotide phosphates interact with R guanidinium or K amino groups; they are H-bonds, when OH or NH interacts with O or N; hydrophobic contacts, when a hydrogen bound to a carbon or a carbon not involved in a carboxyl is involved in interactions; the Van der Waals type was assigned to the other contacts. The program CaPTURE (Gallivan) (Cation–π Trends Using Realistic Electrostatics) was used to identify interactions between the cationic group of lysine and arginine and the aromatic ring of tryptophan.

2.6. Binding energies

Three parameters are calculated, Mean Force Potential (MFP; ΔG), electrostatic energy (ΔE) and partner contact surface areas. Energy gains are calculated taking into account all molecules (solutes and water). They concern direct atom contact with a cut off of 0.6 nm for coulomb term (ΔE) and, more interactions with a larger cut off of 1 nm for Mean Force Potential (MFP) values (ΔG) to take into account the hydrophobic collapse as detailed in Thomas et al. in 2010 [53].

Three systems are evaluated; the solvated complex and the two solvated substrate partners. Molecules are solvated by 3 layers of all-atom water molecules with a dipole moment of 1.85 D units. For the siRNA/CADY interactions, the complex is the siRNA–CADY complex, substrate partners are the siRNA and the whole CADY cage, respectively. For the CADY cage, the complex is the cage with no siRNA, substrate partners are every CADY and the cage made by the other CADYs, respectively. The model of CADY before dynamics is used as a substrate to take into account CADY structural changes. The energies of interaction are half the difference between the complex energy and the sum of the two substrate partners' energy. The contact surface area between partners is half the difference between the sum of the water accessible surface area (ASA) of the two partners minus the water ASA of the complex.

3. Results

3.1. Free CADY and siRNA

3.1.1. CADY

The sequence of CADY has three particularities (Table 1); first, the presence of numerous bulky residues with especially four tryptophans (W3, W7, W14, W18) whereas the few small residues (G1, A5 and A20) are on peptide extremities. The second particularity is the high number of charges with five positively-charged residues (R4, R8, R11, R15 and K19). Moreover, cation–π interactions can be formed between the cationic group of lysine or arginine and the aromatic rings of tryptophan. The third is the occurrence of a motif of four residues (XLWR(K), X being G, A, S and L) repeated four times. Due to the regularity of the motif, an α helix structure optimally

segregates the charged residues (R and K) away from the hydrophobic ones (W and L) but at the same time, the helix gets charged side-chains spatially close leading to an electrostatic repulsion.

The 50 PepLook models of lower energy of CADY in water (Fig. 1A) have close MFP values with an average of -147 ± 8 kJ/mol, well under the -272 kJ/mol per aa stability value of proteins as usual for peptides [53]. Their secondary structures are mainly random coil with a short helical fragment in the center or the N-side of the peptide. This is all, as far as similarities are concerned since fitting the 50 models on the Prime (the best model) gives an averaged Cα RMS deviation of 4.3 ± 0.8 Å indicating a large diversity of three-dimensional configurations. These data support the conclusion that CADY in water is poorly helical and exists as a disordered population since structurally-different conformations have close MFP values. It has been previously shown by circular dichroism that CADY is random coil in water and adopts a more helical conformation in the presence of DOPG or DOPC vesicles and of siRNA [10,14,54]. An increase in helicity is also true in PepLook. When calculations are made in the negatively-charged interface, the 50 models of CADY (Fig. 1B) are more helical with an optimal helicity around 60% in the ten best models. The calculation in the interface goes with a restriction of the structural diversity since the RMS deviation of the 50 interfacial models is reduced to 3.6 ± 1 Å.

The evolution of free CADY was analyzed for 50 ns runs of molecular dynamics in water (Table 2). The RMSD vary rapidly to reach a plateau at 0.6 and 0.8 nm after 20 ns for the helix and the interfacial PepLook models, respectively (Fig. 2A). To make these U shapes, few hydrophobic residues, leucines and also tryptophans get spatially close building small hydrophobic cores. Charged residues are turned outside (Fig. 3) and can form cation–π stacking with tryptophans (in average for 50% of W). To follow the formation of the U shape, the distance between the Cα of the first and last leucines of CADY (L2 and L16) has been recorded (Fig. 2C). With the helix model of CADY a U shape is also rapidly formed and then, opens and closes back between 10 and 20 ns. The disorder of CADY noticed in the structural diversity of PepLook low energy models is illustrated in the dynamics by the instability of CADY and by the different best models obtained from separate runs (Fig. 3). One point is however to be noticed, although highly charged, CADY in water looks always hydrophobic. The isopotential surface around CADY demonstrates this hydrophobicity (Fig. 1). We have previously shown that soluble proteins have equivalent hydrophobic and hydrophilic surfaces [14].

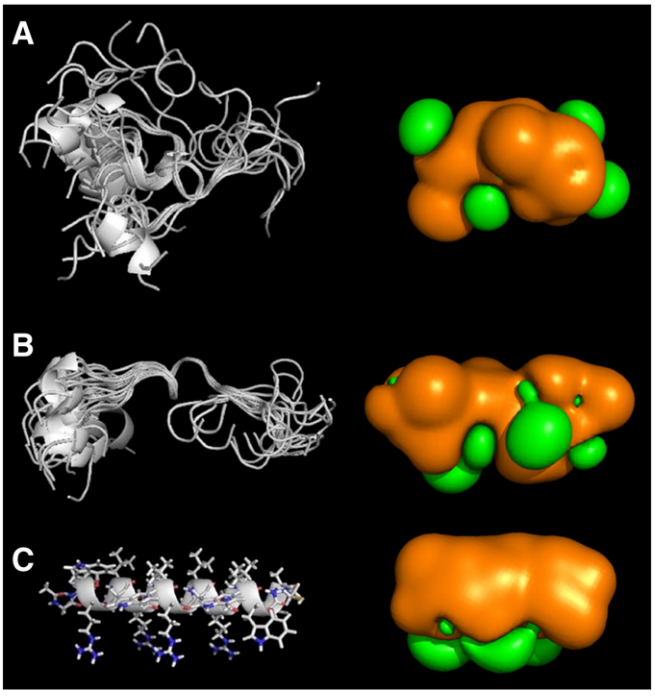

Fig. 1. Models of CADY. (A) Left: the 20 best PepLook models in water were fitted on the Prime (best model). Fitting is made on the central RLLR fragment. Right: the molecular hydrophobicity isopotential (MHP) surfaces (±0.4 kJ) of the Prime. Green surface is hydrophilic, brown is hydrophobic. (B) Models calculated at a DOPG:DOPC membrane interface with PepLook, legend is the same as for A. (C) Helix model, on the left the ribbon and stick representation, on the right the MHP surfaces.

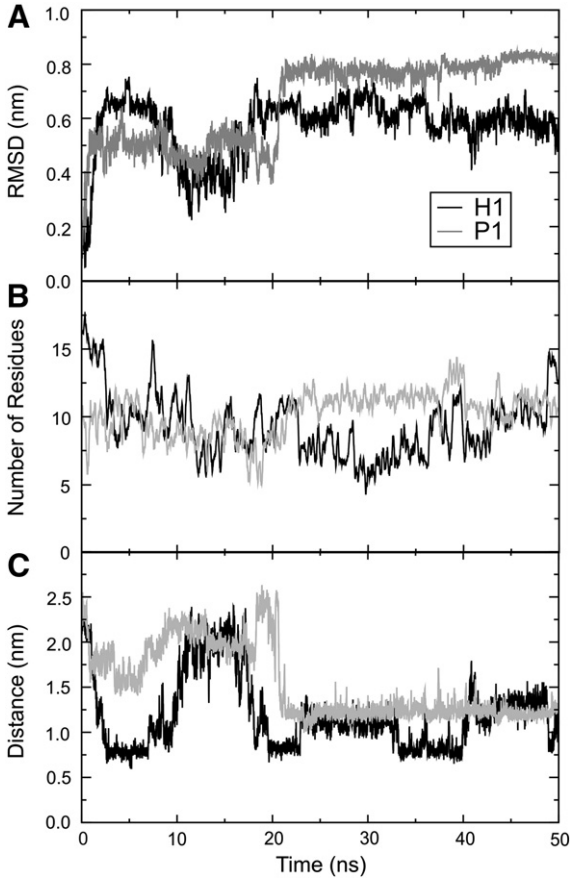

Fig. 2. Dynamics of CADY in water. (A) Variation of RMSD calculated on α-carbons after a least-square fit on the initial structures. (B) Number of residues in helix (average over 21 steps) computed with DSSP along the trajectories. (C) Variation of the distance between the Cα of L2 and L16. Results are presented for the first molecular dynamic carried on with the helical model (H1) and the interfacial PepLook model (P1) of CADY.

3.1.2. siRNA

Where CADY is positively charged, siRNAs are negatively charged with 36–40 phosphate moieties. Unlike CADY, siRNAs are very hydrophilic with ratios of hydrophobic to hydrophilic water-accessible surface of 0.24 and 0.4 for siRNA2 and siRNA1, respectively. siRNA1 is extracted from a complex with four helical peptides in which two peptides are bound in the siRNA groove that is wider than the groove of the siRNA2 explaining the difference of hydrophobicity. Globally, free siRNAs are cylinders of about 2×5–8 nm with a water accessible surface around 80 nm^2. siRNA2 has been studied by molecular dynamics (data not shown) and has similar movements in the solution as in the complex. These results are presented below.

3.2. CADY–siRNA complexes

In bench assays, siRNA and CADY form a complex in low salt water solutions using a molar ratio of 1 nucleic acid for up to 40–80 peptides. In silico, we calculated the binding of CADYs to a molecule of

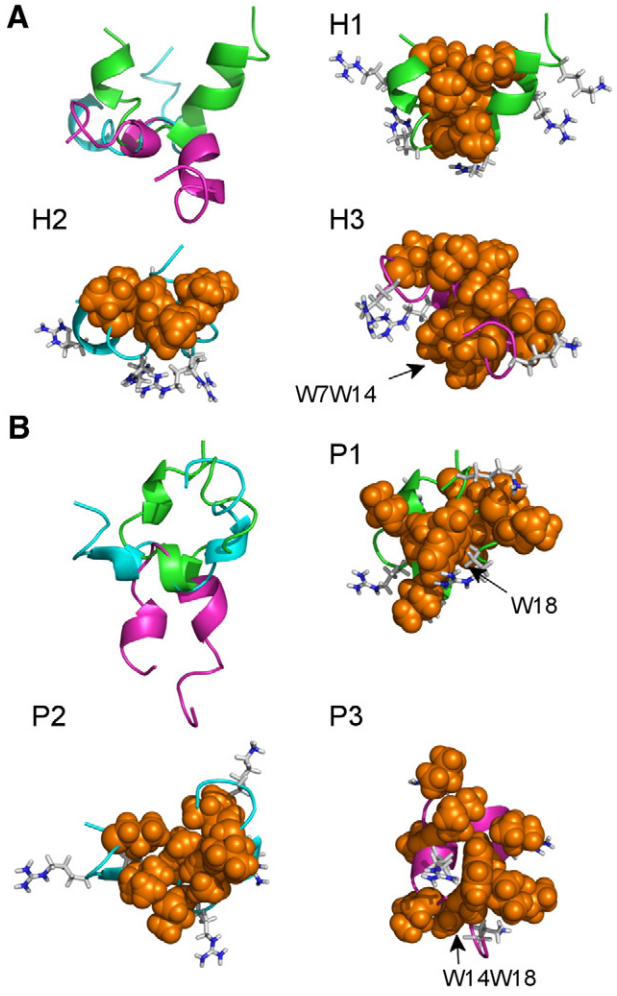

Fig. 3. CADY structures at the end of the molecular dynamics. The models obtained at the end of the three runs that started from (A) the helical model (H1 to H3) and (B) the interfacial Peplook model (P1 to P3) are presented. They are fitted on the RLLR backbone fragment as in Fig. 1 and shown as a backbone cartoon of three different colors to highlight the U shape. Then every model is detailed (right and under) to show the protruding charged residues (sticks) and the residues involved in the core (orange spheres). These residues are leucines and, when indicated, tryptophanes.

siRNA in water up to the inaccessibility of the nucleic acid and further up to 40 CADYs per siRNA.

Since CADY exists as a population of conformers, chances are low that all models that will bind will have the same conformation. To test whether this point is important, we used different 3D models of CADYs and compared the resulting complex structure and energy of interactions. As mixtures are experimentally prepared in water or in diluted phosphate buffers, the PepLook Prime model of CADY in water was used for one series. CADY is known to change the conformation in the presence of siRNA and membranes, i.e. when it faces a charged interface [14]; thus the PepLook amphipathic model of CADY calculated in a charged membrane interface was used in a second series. Further considering the experimental fact that helicity of CADY increases in the presence of siRNA [14], we also calculated the complexes using α helix model of CADY. CADY can bind any siRNA and, in our assays targets of CADYs were the two models of siRNAs described before. Then we calculated six different molecular complexes by using three models of CADY and two different siRNAs. The formation of complexes was followed by the evolution of the accessibility of partners.

3.2.1. Decrease of siRNA and CADY accessible surface in complexes

In Fig. 4, the accessible surface of siRNA progressively decreases with the addition of CADYs and remains constant when 15–17 CADYs are bound. The profile was similar for all the complexes although the number of peptides needed to reach the plateau varied from 13 to 17 (mean is 14 ± 1). It suggests that an average of 14 ± 1 CADYs can have a direct access to the molecule of siRNA. Partial burial of CADYs in complexes also occurs, but with a different course. The binding of the first 5–7 CADYs results in a low decrease of their accessible surface to water. These first CADYs are bound to siRNA and dispersed on the nucleic acid surface. The addition of more peptides results in a linearly constant decrease in the CADY accessible surface especially after the binding of the first 15–17 peptides. In that second phase, the accessible surface of siRNA does not change, supporting the conclusion that CADY burial is essentially due to the onset of CADY–CADY interactions and the building of a "CADY cage". All together, the binding of the different models of CADYs transforms the elongated siRNA helix (length of 5–8 nm; width of 2 nm) into globular complexes of about 7–12 nm (13–38 CADYs).

3.2.2. CADY–siRNA interactions

As expected, the residues implicated in the direct CADY–siRNA interactions are arginines and the siRNA partners are the phosphate moieties (Fig. 5). CADYs implicate at least one but never all their arginines in interaction with the siRNA irrespective of the peptide model used. With the helix model of CADY that displays all the charged residues in the same side, it is the curvature of the siRNA helix that impairs their simultaneous binding. For the water and interfacial models that have arginine pointing out in diverse directions, bound arginines can be from the N-, from the central or from the C-part of CADY. This together with the numerous phosphate groups of siRNA

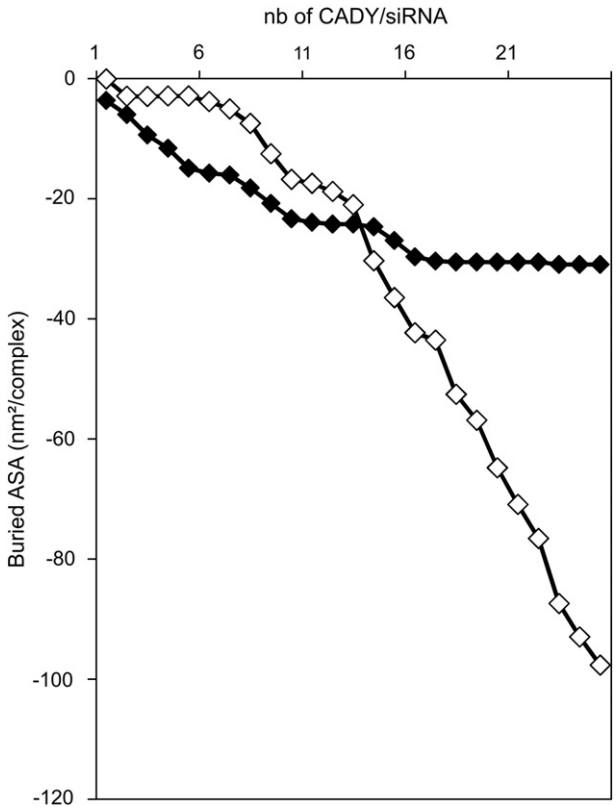

Fig. 4. Variation of siRNA and CADY water accessible surfaces in a complex. The complex was made by the addition of the interfacial PepLook model of CADY to the siRNA1. Black squares represent the siRNA surface area buried by the addition of CADYs. White squares are the CADY accessible surface area buried by CADY–CADY contacts.

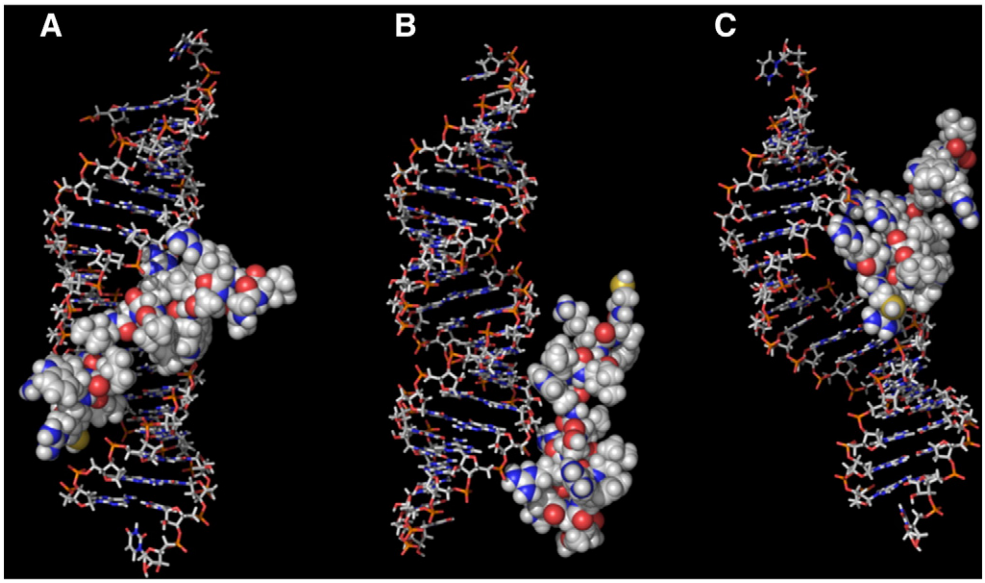

Fig. 5. The first Cady bound to siRNA in three different complexes. (A) The interfacial Prime model of CADY with siRNA1. (B) The interfacial Prime model of CADY with siRNA2. (C) The water Prime model of CADY with siRNA1.

results in numerous and diverse possibilities for the positioning of CADY at the surface of siRNA. One particular position is obtained with siRNA1 that accepts a peptide in its enlarged groove (Fig. 5A) ensuring both electrostatic interactions of arginine with the phosphate in the siRNA crest and more hydrophobic contacts in the groove. More frequently, CADYs are restricted to external positions and to electrostatic interactions. They are positioned either in line with the siRNA phosphate crest or are bridging two crests as in models B and C of Fig. 5. It is important to notice that arginine-phosphate salt bridges are "non-selective" of siRNA sequences because phosphate alignments are in any siRNA sequence.

3.2.3. Complex disorder and stability

We have analyzed the evolution of four complexes during molecular dynamic runs (Table 2). These complexes have one and two layers of CADYs and were made from siRNA2 and from two different models of CADY, the interfacial PepLook Prime and the α helix. During the dynamic runs, the A form of siRNA2 undergoes small variations as compared to those of CADY. The nucleic acid helix has a stretching movement on its length but no unmatching of strands with deviations of RMS between 0.3 and 0.4 nm (Fig. 6A) essentially attributed to fluctuations of the major groove widths as evaluated by measuring the distance between several pairs of phosphates (Fig. 6B). The mean width is around 1.5 nm and fluctuates between 1 and 2 nm. All bases are and remain matched. The siRNA length, as evaluated by the distance between P2 and P18 varies between 4 and 5 nm. CADYs remain attached to the phosphates, change conformations but do not tend to insert in grooves. Every CADY has a different evolution (Supplementary Fig. S1); some have little variations with low RMS deviations (0.2–0.3) with respect to the initial conformation, while others have wider movements (RMSD 0.7–0.8) (Fig. 6A). When the initial model is α helical, CADY conformation is less changed during the dynamic runs of the one and two layer complexes than when the initial model is the interfacial Prime model of PepLook (Figs. 6C, 7 and Supplementary Figs. S1–S4). The movements of CADY in complexes are always more restricted than the movements of CADY in water (Supplementary Fig. S1 to be compared to Figs. 1 and 2). This supports the idea that in complexes, the movements are restricted in their magnitude and in their direction by the interactions with the nucleic acid and with the other CADYs. During the dynamics, the contact surface area between the siRNA and CADY increases to around 30 nm^2 for the complexes with one layer of CADYs and slightly less for the other complexes. Meanwhile, the complex water-accessible surfaces decrease (Fig. 6D). These decreases are explained partly by the increases of the surface of contact between siRNA and CADYs and mostly by the increases of the surface of contact between peptides (Fig. 6D).

3.2.4. Energy balance of siRNA–CADYs complexes

To further compare the CADY–siRNA complexes and to evaluate their evolutions during the dynamics in water, we calculated the binding energy terms (ΔE (electrostatic) and ΔG (MFP)) taking into account the cost of partner desolvation and structural changes. We also evaluated the contact surface areas. During the dynamics, the flexibility of CADY improves and increases the interaction between the phosphates and arginines. This results in an increased gain of electrostatic energy (-280 ± 4 kJ/mol per nm^2 for CP1 as compared to -209 ± 13 kJ/mol per nm^2 prior to the dynamics) but essentially in an increase of the surface of contact between CADYs and siRNA (42 nm^2 for CP1 as compared to 25 nm^2 per siRNA prior to dynamics) (Table 3). Meanwhile, the electrostatic contribution of CADY–CADY contacts is and remains low (-38 ± 25 kJ/mol per nm^2 prior to and -46 ± 21 kJ/mol per nm^2 after the CP1 dynamics). During the molecular dynamics, there is repulsion between R positive charges and only few of them are within the cut-off of 0.6 nm.

CADY movements also result in an increase of MFP gains due to an improvement of the complex collapse as demonstrated by the decrease of the water accessible surface area of both, the one and two layer complexes and, consequently by the increase of the surface of direct contacts between the partners (for CP1, there is a 68% increase for the siRNA–CADYs contacts and a 282% increase for the CADY–CADYs contacts) (Table 3). The contribution of the CADY–siRNA contacts to the hydrophobic collapse is poor (ΔG was only -21 ± 17 kJ/mol per nm^2 prior to and is -71 ± 4 kJ/mol per nm^2 after the CP1 dynamics). The contribution of CADY–CADY contacts is larger and depends on the number of CADYs in the cage. However, expressed by a unit of contact surface, it was 0 ± 259 kJ/mol per nm^2 prior to the CP1 dynamics and is -568 ± 117 kJ/mol per nm^2 after the dynamics. This supports

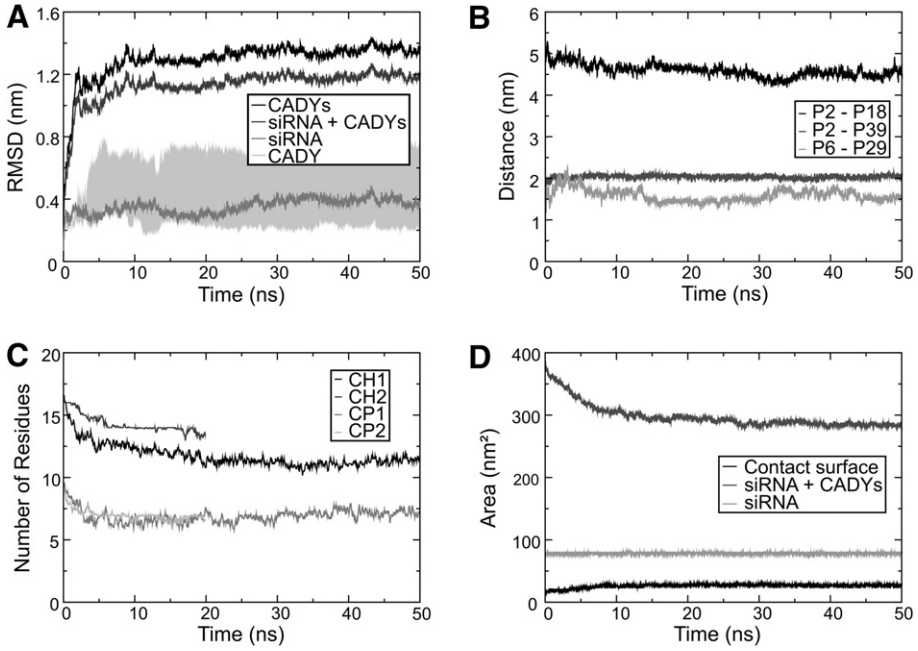

Fig. 6. Evolution of different parameters during the molecular dynamics of the complexes. (A) RMSD calculated on α-carbons and/or phosphorus atoms after a least-square fit on the initial complex structure. (B) Distances between phosphorus pairs representing the siRNA length (P2–P18), the matching of siRNA base pairs (P2–P39) and the major groove width (P6–P29). For the sake of clarity, only three pairs are shown. (C) The number of helical residues of CADY averaged over 21 steps computed with DSSP along the trajectories. (D) Accessible surface of the complex, the siRNA2 and, the contact surface between siRNA2 and CADYs. Graphs from panels A, B and D are derived from the one layer complex made with the helical model of CADY and siRNA2 (CH1).

the conclusion that most hydrophobic interactions in the complexes are in the peptide cage.

3.2.5. Detailed analysis of molecule contacts

To further characterize the CADY–siRNA interactions after the molecular dynamics, atomic contacts were detailed. Fig. 8 gathers the number of the CADY–siRNA contacts in all the complexes (Fig. 8A and D) and details their distribution in the one-layer complex made from the interfacial PepLook model of CADY (CP1, Fig. 8C). CADYs interact with the siRNA mainly through R residues (53 to 75% of all the CADY–siRNA contacts in the different complexes) (Fig. 7 and Supplementary Figs. S2–S4). Arginines make salt bridges with the RNA phosphate groups (52% of the R–siRNA contacts) and hydrogen bonds with oxygens of sugars and bases (19% of the R–siRNA contacts) (Fig. 8C). Fig. 8D shows that CADYs in the one layer complex made with the interfacial model of CADY has more contacts with the nucleotide bases than with sugar, due to more arginine residues implicated in the H-bonds and Van der Waals interactions. The backbone atoms of CADY are also implicated in the H-bonds with siRNA (30% of all H-bonds). Regarding the position of CADYs on the siRNA2 surface, no peptide was and has been inserted into the major groove before and during the dynamics.

The CADY–siRNA interactions also involve hydrophobic and Van der Waals contacts between amino acid side chains and nucleotide sugar and bases (9 and 20% of all contacts). These contacts arise mainly in the minor groove (70%). There is almost no difference between the one and two layer complexes. More CADY–siRNA interactions are involving W when complexes are formed from the helix model of the peptide.

Regarding the panel of residues implicated in the CADY/CADY interactions, hydrophobic contacts between the side chains are major (63% of all the contacts, Fig. 8C) and L and W play a major role (Fig. 8B). The H-bonds are formed between NH of R and W and backbone carboxyl. The cation–π stacking interaction between W and R or K of the different peptides also arise for 6 (CH1), 13 (CH2), 9 (CP1) and 14% (CP2) of the W. Comparing the one- and two-layer complexes emphasizes the increased frequency of the hydrophobic and cation–π stacking interactions in the larger complex cages. In conclusion to the analysis of the complexes, the 3D conformations of CADYs change during the dynamics to stabilize the complexes by increasing the electrostatic contribution of the CADY–siRNA interactions, by enlarging the hydrophobic collapse of CADYs in the cage and by locking complex structures with H-bonds and cation–π stacking (Fig. 8E and F). The main parameters of complexes of similar sizes i.e. the contact ASA per CADY and per siRNA, the accessible surface of the complexes are similar irrespective of the initial CADY and siRNA models used.

3.3. Structure–function relationships of complexes

Biological assays have demonstrated that active mixtures of CADYs and siRNA require a minimum of 10–15 peptides per siRNA [10,14]. According to the modeling data, the 15:1 ratio is a one-layer complex, thus the 10:1 ratio should be a complex with a partial layer of CADYs. CADY has 5 positive charges and siRNAs 36 to 40 negative charges; hence the 10:1 complex is positively charged. Charges could be important to locate the complex at the membrane surface and to trigger its transfer into the cell.

Biological assays have also demonstrated that higher CADYs/siRNA ratios give more stable preparations and, ratios of 40:1 and over are optimal. Thirty four to thirty eight CADYs make two layers of peptides around the nucleic acid supporting the conclusion that the experimental 40:1 ratio corresponds to the two-layer complexes. Again, these complexes are positively charged. Arginines are numerous at the surface of complexes (Fig. 7 and Supplementary Fig. S4) and charges should be important for the interactions with the negative charges of membrane lipids and of cell sugar coats.

This raised the question of the higher stability of larger complexes with respect to structural parameters. The average MFP value of stable globular proteins is −271 kJ/mol per aa [53] irrespective of their folds. The MFP value (kJ/mol per aa) of the CADY cage is never as low and is at best 63 to 69% of that value. This supports the conclusion that, even the large CADY cages are not as stable as the proteins. This could be important to facilitate the dynamic story of the complex, i.e. its entry and unwrapping in cells. The one and two layer complexes differ in their apparent capacity to adapt to the external

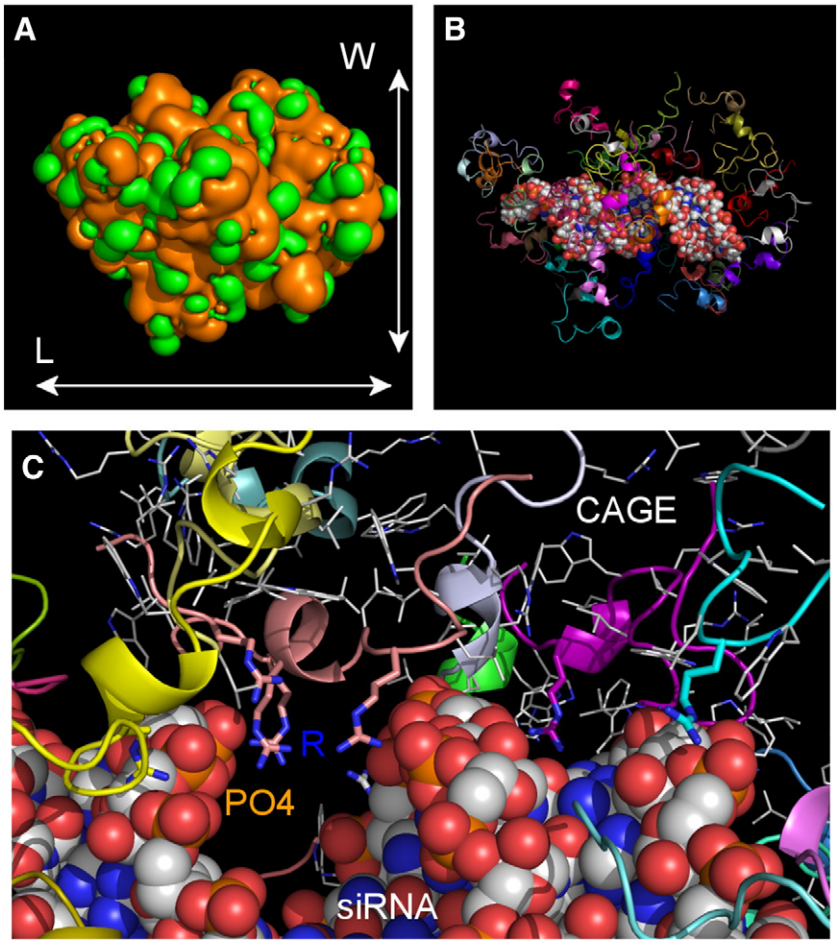

Fig. 7. CADY–siRNA complex after the molecular dynamics (CP2). The complex is the two layer complex made with the Peplook interfacial Prime as the initial CADY model. (A) MHP surfaces of the complex with L and W defined as the length and width of the complex (L = 11 nm and W = 8 nm). (B) The complex with CADY in a cartoon representation. (C) Illustration of the peptide cage and the siRNA interface. CADY backbones are cartoons with residue side chains in strings (L, W, K and R). Few arginines pointing towards PO4 are shown in sticks. siRNA atoms are in the sphere representation; Hydrogen and peptide backbone atoms are hidden.

medium. During the formation of a complex, a very hydrophilic siRNA (hydrophobicity ratios of the two siRNAs are 0.24 and 0.4) is covered by hydrophobic CADYs. Resulting complexes have similar or higher (up to 1.4) hydrophobicity ratios than CADY. The hydrophobicity ratio of 1 is characteristic of the soluble proteins [50]. When complexes are relaxed by the dynamics in water, the movements of CADY improve the interactions within the complexes and also the interactions with the solvent. The hydrophobicity ratios of the complexes with a single layer of CADYs were 1.22–1.28 before the dynamics and decrease to 1.17–1.18 after the dynamics in water. For the two layer complexes, the values were 1.31 and 1.27 and decrease to 1.02 after the dynamics in water. Hence, the large cage of CADYs seems more efficient to adapt the cage surface to the water medium.

4. Discussion

Although the therapeutic applications of CPP in the transfer of non-permeant drugs are promising, the structure of the CPP–cargo complex and the molecular mechanisms of the membrane translocation are unclear [7,23,24,55,56]. In this paper we use molecular modeling

Table 3
CADY–siRNA complexes before and after the molecular dynamics.

Simulation name[a]	Complex ASA (nm^2)	Hydrophobicity ratio	Contact surface with siRNA (nm^2)	Contact surface between peptides (nm^2/CADY)[b]	ΔE kJ/mol per nm^2 (with siRNA)[b]	ΔG kJ/mol per nm^2 (with siRNA)[b]	ΔE kJ/mol per nm^2 (between peptides)[b]	ΔG kJ/mol per nm^2 (between peptides)[b]
CP1 (BD)	431	1.22	25	1.7 ± 1.6	−209 ± 13	−21 ± 17	−38 ± 25	0 ± 259
CP1 (AD)	290	1.17	42	6.5 ± 1.4	−280 ± 4	−71 ± 4	−46 ± 21	−568 ± 117
CP2 (BD)	726	1.31	20	3.3 ± 1.7	−171 ± 13	0 ± 0	−17 ± 21	−38 ± 155
CP2 (AD)	506	1.07	39	7.3 ± 1.9	−309 ± 8	−84 ± 8	−67 ± 38	−539 ± 67
CH1 (BD)	403	1.28	20	1.7 ± 1.3	−188 ± 8	84 ± 21	−17 ± 21	4 ± 251
CH1 (AD)	255	1.17	40	7.9 ± 1.6	−276 ± 4	−75 ± 4	−59 ± 13	−376 ± 113
CH2 (BD)	703	1.27	24	3.7 ± 2.0	−167 ± 17	42 ± 38	−13 ± 25	−364 ± 155
CH2 (AD)	488	1.02	34	8.2 ± 2.9	−322 ± 13	−146 ± 17	−63 ± 29	−523 ± 79

[a] BD corresponds to complexes prior to dynamics and AD after dynamics.
[b] Standard deviations are given in brackets.

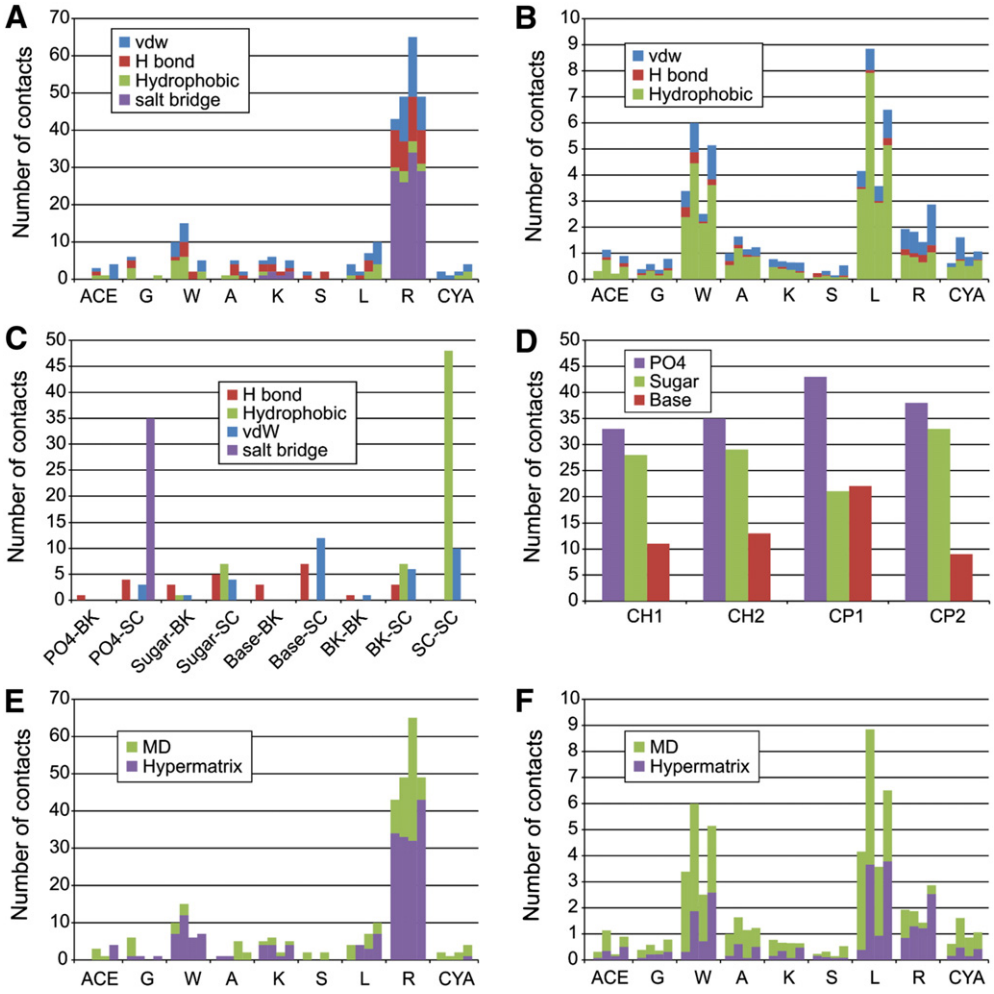

Fig. 8. Analysis of the CADY–siRNA and CADY–CADY interactions. (A) Number of contacts between CADY and the siRNA per amino acid type and the interaction type. Contacts for each complex are represented, first bars correspond to CH1, second to CH2, third to CP1 and fourth to CP2. (B) Number of contacts between different peptides as a function of the amino acid type and the interaction type divided by the number of peptides in the complex. (C) Number of contacts between CADY and the siRNA according to their localization (backbone BK or side chains SC for CADY and phosphate PO4, sugar or base for siRNA) and the interaction type in the one layer complex made with the interfacial PepLook model of CADY and the siRNA2 (CP1). (D) Contact localization on the siRNA. (E) Number of contacts between CADY and the siRNA per amino acid type before (Hypermatrix) and after molecular dynamics (MD). (F) Number of contacts between different peptides as a function of the amino acid type before and after the molecular dynamics. The contacts of atoms were counted using a distance cutoff of 0.35 nm for the final structures of the molecular dynamic simulations. ACE and CYA stand for the acetyl and the cysteamide moieties, respectively.

algorithms to calculate CADY and the non-covalent complex of CADYs with its current cargo (siRNA) in water. We screen several options through the different 3D models of CADY and a range of CADY/siRNA ratios that cover biological data. In the case of CADY, current biological assays support that at least 10 to 15 CADYs/siRNA are required to succeed in a siRNA transfer and, the complexes presenting the best stability recruit of about 40–80 peptides per siRNA.

Up to now, molecular modeling analyses of CPP were dedicated to structure predictions [14,33] and to peptide/membrane interactions [29,31]. The binding of a CPP to a cargo is another, yet the unexplored process and, complexes were never calculated likely due to the complexity of the task. Indeed, no experimental model of CADY has been resolved to start from and the complexes are very large. In the discussion, we shall emphasize the essential structural particularities of CADY, will analyze the complexes obtained from the screening approach with rigid models and the complexes relaxed by molecular dynamics to finally evaluate their common particularities and, the relevance and limits of our approach.

Regarding structure predictions, the 50 low-energy models of CADY in water are mainly random coil with similar low MFP values. There is some differences of the secondary structures but, essentially large fluctuations of the 3D structures as assessed by their RMS deviations (around 4 Å). This supports the conclusion that the CADY structure is poorly self-stable and is in agreement with the structure fluctuations reported in the experimental evaluations [54]. CADY forms U shapes in water implicating few hydrophobic residues in a small core. The U shapes of CADY are hydrophobic further explaining the poor stability of the peptides in water. The constant hydrophobicity of the CADY models in water is in agreement with the fact that the peptide inserts in the membranes and we suggest that it explains why CADYs continue to bind when siRNA is no longer accessible. In those specific conditions resulting in the formation of a second layer of peptides, the driving force for the CADY binding cannot be electrostatic. It should rather be the preference of free CADY for a hydrophobic surface (the one layer CADYs–siRNA complex) than for the water solution. This should be especially true with the high concentrations of CADY and siRNA that were used to prepare the vector and might also explain why the unitary complex further aggregates to form raspberry-like nanoparticles [50]. The experimental data also report that CADY helicity increases with the presence of siRNA and membranes [54]. The whole α helix conformation with all arginines on one side and leucine and tryptophan residues on the opposite side that we used in one of our series is very amphipathic. Nevertheless, this α helix model is not found among the 50 best models of PepLook

supporting that its probability of occurrence is low, as experimentally suggested.

It is clear that due to its structural polymorphism, the models of CADY in solutions are diverse. Moreover, the sequence of CADY is a repeat of the XLWR motifs where arginine is the binding element to siRNA giving several possible binding options. On the other side, siRNA has 36 to 40 phosphate groups that can all be binding targets. It is clear that expecting a unique model of the complex is utopian and explains the difficulties met in the experimental attempts to resolve the complex structure. Hence the modeling calculations appear as an interesting mean to explore the main parameters of the complex formation. The numerous possibilities make an exhaustive screening impossible. We chose to use conditions testing a large panel of possibilities, to start from rigid models of CADY and of siRNAs and, to go to dynamic movements later on. Indeed, one of the aspects of our approach is to provide PDB models suitable for running molecular dynamics. Such dynamics would have been impossible from the free molecules of siRNA and CADY. Nevertheless, the dynamics data are essential to demonstrate the role of the CADY disorder in the complex stability.

Since the initial binding of CADYs is an electrostatic interaction with the nucleic acid, eight CADYs could have been sufficient to neutralize the 36–40 phosphates of a molecule of siRNA. We start from the different 3D models of CADY and find that 14 ± 1 peptides are required to cover the nucleic acid. In Konate et al. 2010, CADY/siRNA interactions have been titrated and saturation occurs at a peptide/siRNA molar ratio of 12 ± 2 [14]. Hence, the agreement between the experimental assays and our data supports that the approach is relevant and that CADYs do not bind all their arginines. Finally, the saturation of the siRNA surface generates positively charged complexes due to the excess of CADY charges. These positive charges could be important for the attachment of the complex to the membrane.

The cysteamide residue, which has been shown to improve the cellular uptake, should not assume a specific function during the complex building. Though disulfide bridges could form between two cysteamide residues as this has been observed for other cell penetrating peptides under oxidizing conditions [57,58], CADY remains monomeric in the solution (data not shown). Moreover, the CADY peptide with no cysteamide has also been characterized in vitro. It is as efficient and presents the same properties as CADY with a cysteamide residue in the solution and in the complexes. The complexes were therefore calculated from the monomeric CADYs.

The complexes were prepared from the three models of CADY, the Prime model of PepLook in water, in a membrane interface and all the helix models. In all cases, the electrostatic interactions of the arginine side chains with the siRNA phosphates are the driving force for the binding of the first layer and the poor implication of the nucleic acid bases explains the non-selectivity of CADY for siRNA sequences.

The energies of interaction in the complexes were estimated after taking the cost of the partner desolvation and conformational changes into account [59]. The values indicate that salt bridges play the major role in the siRNA–peptide interaction. In the second layer of complexes, the peptides have no contact with the nucleic acid and the cage is stabilized by the CADY–CADY hydrophobic interactions. These interactions are clearly optimized by the disorder of CADY. As discussed before, we also suggest that the binding of the second layer is triggered by the free peptide hydrophobicity. The correlation between energies of the atom interactions in the complexes and the biochemical values of affinity, of specific activity and binding capacities should be very useful but is not obvious. The dissociation constant of CADY and siRNA was evaluated at 15–47 nM [10,14]. In the models, the CADY and siRNA molecules have an optimal surface of contact around 40 nm^2 per complex and an electrostatic energy gain of -297 ± 21 kJ/mol per nm^2. The simulations carried out on the different complexes converge on the fact that the contact surfaces between siRNA–CADY and CADYs increase due to the CADY disorder. Finally, all the complexes have similar values of the contact surface and of the energy supporting the conclusion that those values are a signature of the siRNA–CADY complexes. In addition, the disorder of CADY facilitates the onset of the H-bonds: such bonds are less energetic than the salt bridges but require precise positions of the H-donor and acceptor and thus are likely to participate in locking the 3D structures. Besides the H-bonds, the complexes are also stabilized by the formation of the cation–π stacking interactions between R and W which are the two constitutive residues of CADY.

The structural polymorphism of CADY is also responsible for the fact that the accessible surface of the larger complexes can reach the hydrophobicity ratio value of 1 in water i.e. the standard ratio value of the soluble proteins [50]. The single layer complexes do not have this capacity and remain hydrophobic after the dynamic runs. Movements of CADYs in that single layer must be restricted by the binding of its polar residues to the siRNA phosphate, whereas in the second layer, the polar residues of CADYs have less restriction of movement. This supports the suggestion that a minimal cage of two layers is necessary for an optimal adaptability of the complexes to water. It also opens to the suggestion that will be tested in future studies that a direct uptake of the complexes across the plasma membrane could require the unwrapping of the second layer as proposed by Konate et al. [14]. This would result in more hydrophobic smaller complexes and is already supported by the instability of the two layer complex in a hydrophobic solvent (unpublished data).

In conclusion, we calculated the non-covalent CADY–siRNA complexes by a molecular modeling screening approach and analyzed their dynamic behavior in water. The arginines of the first layer of peptides bind to the crest of the siRNA phosphate as previously supported [10,14] and the partner interactions hardly implicate the nucleic acid bases explaining the absence of selectivity of CADY for siRNA sequences. Due to the occurrence of several binding residues per CADY and to the numerous binding targets in siRNA, the structural combination of the CADY positions in siRNA results in numerous possibilities of the complex structures. Saturating the siRNA accessible surface with a layer of 12 ± 2 (experimental titration) or 14 ± 1 CADYs (this study) gives hydrophobic though positively charged one-layer complexes. When the first layer of CADYs is bound, CADYs continue to bind because the peptide is poorly stable in water. A CADY–siRNA ratio of 40:1, which gives stable therapeutic vector preparations, leads to complexes with a second layer of CADYs in which the peptide's spontaneous movements stabilize the cage by amplifying its hydrophobic collapse and by regulating its interactions with the external partners. The complexes are 7–12 nm particles, they are much smaller than the 70–80 nm raspberry-like nanoparticles as seen by electron microscopy [23]. They should however be the unitary element of those raspberry-like nanoparticles.

Supplementary data to this article can be found online at http://dx.doi.org/10.1016/j.bbamem.2012.09.006.

References

[1] S.B. Fonseca, M.P. Pereira, S.O. Kelley, Recent advances in the use of cell-penetrating peptides for medical and biological applications, Adv. Drug Deliv. Rev. 61 (2009) 953–964.
[2] D. Castanotto, J.J. Rossi, The promises and pitfalls of RNA-interference-based therapeutics, Nature 457 (2009) 426–433.
[3] C.V. Pecot, G.A. Calin, R.L. Coleman, G. Lopez-Berestein, A.K. Sood, RNA interference in the clinic: challenges and future directions, Nat. Rev. Cancer 11 (2011) 59–67.
[4] K.A. Whitehead, R. Langer, D.G. Anderson, Knocking down barriers: advances in siRNA delivery, Nat. Rev. Drug Discov. 8 (2009) 129–138.
[5] A. de Fougerolles, H.P. Vornlocher, J. Maraganore, J. Lieberman, Interfering with disease: a progress report on siRNA-based therapeutics, Nat. Rev. Drug Discov. 6 (2007) 443–453.
[6] G.P.H. Dietz, M. Bahr, Delivery of bioactive molecules into the cell: the Trojan horse approach, Mol. Cell. Neurosci. 27 (2004) 85–131.
[7] F. Heitz, M.C. Morris, G. Divita, Twenty years of cell-penetrating peptides: from molecular mechanisms to therapeutics, Br. J. Pharmacol. 157 (2009) 195–206.

[8] P. Jarver, I. Mager, U. Langel, In vivo biodistribution and efficacy of peptide mediated delivery, Trends Pharmacol. Sci. 31 (2010) 528–535.
[9] L. Crombez, M.C. Morris, S. Dufort, G. Aldrian-Herrada, Q. Nguyen, G. Mc Master, J.L. Coll, F. Heitz, G. Divita, Targeting cyclin B1 through peptide-based delivery of siRNA prevents tumour growth, Nucleic Acids Res. 37 (2009) 4559–4569.
[10] L. Crombez, G. Aldrian-Herrada, K. Konate, Q.N. Nguyen, G.K. McMaster, R. Brasseur, F. Heitz, G. Divita, A new potent secondary amphipathic cell-penetrating peptide for siRNA delivery into mammalian cells, Mol. Ther. 17 (2009) 95–103.
[11] S.E. Andaloussi, T. Lehto, I. Mager, K. Rosenthal-Aizman, Oprea II, O.E. Simonson, H. Sork, K. Ezzat, D.M. Copolovici, K. Kurrikoff, J.R. Viola, E.M. Zaghloul, R. Sillard, H.J. Johansson, F. Said Hassane, P. Guterstam, J. Suhorutsenko, P.M. Moreno, N. Oskolkov, J. Halldin, U. Tedebark, A. Metspalu, B. Lebleu, J. Lehtio, C.I. Smith, U. Langel, Design of a peptide-based vector, PepFect6, for efficient delivery of siRNA in cell culture and systemically in vivo, Nucleic Acids Res. 39 (2011) 3972–3987.
[12] A. Eguchi, S.F. Dowdy, siRNA delivery using peptide transduction domains, Trends Pharmacol. Sci. 30 (2009) 341–345.
[13] L. Crombez, A. Charnet, M.C. Morris, G. Aldrian-Herrada, F. Heitz, G. Divita, A non-covalent peptide-based strategy for siRNA delivery, Biochem. Soc. Trans. 35 (2007) 44–46.
[14] K. Konate, L. Crombez, S. Deshayes, M. Decaffmeyer, A. Thomas, R. Brasseur, G. Aldrian, F. Heitz, G. Divita, Insight into the cellular uptake mechanism of a secondary amphipathic cell-penetrating peptide for siRNA delivery, Biochemistry 49 (2010) 3393–3402.
[15] M.C. Morris, S. Deshayes, F. Heitz, G. Divita, Cell-penetrating peptides: from molecular mechanisms to therapeutics, Biol. Cell 100 (2008) 201–217.
[16] M.C. Morris, J. Depollier, J. Mery, F. Heitz, G. Divita, A peptide carrier for the delivery of biologically active proteins into mammalian cells, Nat. Biotechnol. 19 (2001) 1173–1176.
[17] M.C. Morris, P. Vidal, L. Chaloin, F. Heitz, G. Divita, A new peptide vector for efficient delivery of oligonucleotides into mammalian cells, Nucleic Acids Res. 25 (1997) 2730–2736.
[18] M.A. Munoz-Morris, F. Heitz, G. Divita, M.C. Morris, The peptide carrier Pep-1 forms biologically efficient nanoparticle complexes, Biochem. Biophys. Res. Commun. 355 (2007) 877–882.
[19] A. Thomas, L. Lins, G. Divita, R. Brasseur, Realistic modelling approaches of structure–function properties of CPP in non-covalent complexes, Biochim. Biophys. Acta 1798 (2010) 2217–2222.
[20] F. Simeoni, M.C. Morris, F. Heitz, G. Divita, Insight into the mechanism of the peptide-based gene delivery system MPG: implications for delivery of siRNA into mammalian cells, Nucleic Acids Res. 31 (2003) 2717–2724.
[21] J.P. Richard, K. Melikov, E. Vives, C. Ramos, B. Verbeure, M.J. Gait, L.V. Chernomordik, B. Lebleu, Cell-penetrating peptides. A reevaluation of the mechanism of cellular uptake, J. Biol. Chem. 278 (2003) 585–590.
[22] R. Brasseur, G. Divita, Happy birthday cell penetrating peptides: already 20 years, Biochim. Biophys. Acta 1798 (2010) 2177–2181.
[23] A. Rydström, S. Deshayes, K. Konate, L. Crombez, K. Padari, H. Boukhaddaoui, G. Aldrian, M. Pooga, G. Divita, Direct translocation as major cellular uptake for CADY self-assembling peptide-based nanoparticles, PLoS One 6 (2011) e25924.
[24] H. Raagel, P. Saalik, M. Pooga, Peptide-mediated protein delivery — which pathways are penetrable? Biochim. Biophys. Acta 1798 (2010) 2240–2248.
[25] C.T. Taylor, G.T. Furuta, K. Synnestvedt, S.P. Colgan, Phosphorylation-dependent targeting of cAMP response element binding protein to the ubiquitin/proteasome pathway in hypoxia, Proc. Natl. Acad. Sci. U.S.A. 97 (2000) 12091–12096.
[26] S. Deshayes, S. Gerbal-Chaloin, M.C. Morris, G. Aldrian-Herrada, P. Charnet, G. Divita, F. Heitz, On the mechanism of non-endosomial peptide-mediated cellular delivery of nucleic acids, Biochim. Biophys. Acta 1667 (2004) 141–147.
[27] D. Derossi, S. Calvet, A. Trembleau, A. Brunissen, G. Chassaing, A. Prochiantz, Cell internalization of the third helix of the antennapedia homeodomain is receptor-independent, J. Biol. Chem. 271 (1996) 18188–18193.
[28] H.D. Herce, A.E. Garcia, J. Litt, R.S. Kane, P. Martin, N. Enrique, A. Rebolledo, V. Milesi, Arginine-rich peptides destabilize the plasma membrane, consistent with a pore formation translocation mechanism of cell-penetrating peptides, Biophys. J. 97 (2009) 1917–1925.
[29] S. Yesylevskyy, S.J. Marrink, A.E. Mark, Alternative mechanisms for the interaction of the cell-penetrating peptides Penetratin and the TAT peptide with lipid bilayers, Biophys. J. 97 (2009) 40–49.
[30] C.M. Dunkin, A. Pokorny, P.F. Almeida, H.S. Lee, Molecular dynamics studies of transportan 10 (tp10) interacting with a POPC lipid bilayer, J. Phys. Chem. B 115 (2010) 1188–1198.
[31] H.D. Herce, A.E. Garcia, Molecular dynamics simulations suggest a mechanism for translocation of the HIV-1 TAT peptide across lipid membranes, Proc. Natl. Acad. Sci. U.S.A. 104 (2007) 20805–20810.
[32] A. Thomas, S. Deshayes, M. Decaffmeyer, M.H. Van Eyck, B. Charloteaux, R. Brasseur, Prediction of peptide structure: how far are we? Proteins Struct. Funct. Bioinforma. 65 (2006) 889–897.
[33] S. Deshayes, M. Decaffmeyer, R. Brasseur, A. Thomas, Structural polymorphism of two CPP: an important parameter of activity, Biochim. Biophys. Acta 1778 (2008) 1197–1205.
[34] S. Deshayes, K. Konate, G. Aldrian, L. Crombez, F. Heitz, G. Divita, Structural polymorphism of non-covalent peptide-based delivery systems: highway to cellular uptake, Biochim. Biophys. Acta 1798 (2010) 2304–2314.
[35] R. Brasseur, V. Cabiaux, J.A. Killian, B. de Kruijff, J.M. Ruysschaert, Orientation of gramicidin A at the lysophosphatidylcholine/water interface: a semi-empirical conformational analysis, Biochim. Biophys. Acta Biomembr. 855 (1986) 317–324.
[36] R. Brasseur, J.A. Killian, B. De Kruijff, J.M. Ruysschaert, Conformational analysis of gramicidin–gramicidin interactions at the air/water interface suggests that gramicidin aggregates into tube-like structures similar as found in the gramicidin-induced hexagonal HII phase, Biochim. Biophys. Acta 903 (1987) 11–17.
[37] P. Ducarme, A. Thomas, R. Brasseur, The optimisation of the helix/helix interaction of a transmembrane dimer is improved by the IMPALA restraint field, Biochim. Biophys. Acta 1509 (2000) 148–154.
[38] I. Martin, M.C. Dubois, F. Defrise-Quertain, T. Saermark, A. Burny, R. Brasseur, J.M. Ruysschaert, Correlation between fusogenicity of synthetic modified peptides corresponding to the NH2-terminal extremity of simian immunodeficiency virus gp32 and their mode of insertion into the lipid bilayer: an infrared spectroscopy study, J. Virol. 68 (1994) 1139–1148.
[39] R.F. Epand, A. Thomas, R. Brasseur, S.A. Vishwanathan, E. Hunter, R.M. Epand, Juxtamembrane protein segments that contribute to recruitment of cholesterol into domains, Biochemistry 45 (2006) 6105–6114.
[40] R.M. Epand, A. Thomas, R. Brasseur, R.F. Epand, Cholesterol interaction with proteins that partition into membrane domains: an overview, Subcell. Biochem. 51 (2010) 253–278.
[41] H.J.C. Berendsen, D. Vanderspoel, R. Vandrunen, Gromacs — a message-passing parallel molecular-dynamics implementation, Comput. Phys. Commun. 91 (1995) 43–56.
[42] P. Emsley, K. Cowtan, Coot: model-building tools for molecular graphics, Acta Crystallogr. D: Biol. Crystallogr. 60 (2004) 2126–2132.
[43] L. Lins, B. Charloteaux, C. Heinen, A. Thomas, R. Brasseur, "De novo" design of peptides with specific lipid-binding properties, Biophys. J. 90 (2006) 470–479.
[44] P. Ducarme, M. Rahman, R. Brasseur, IMPALA: a simple restraint field to simulate the biological membrane in molecular structure studies, Proteins 30 (1998) 357–371.
[45] E.J. Sorin, V.S. Pande, Exploring the helix-coil transition via all-atom equilibrium ensemble simulations, Biophys. J. 88 (2005) 2472–2493.
[46] U. Essmann, L. Perera, M.L. Berkowitz, T. Darden, H. Lee, L.G. Pedersen, A smooth particle mesh Ewald method, J. Chem. Phys. 103 (1995) 8577–8593.
[47] J.P. Ryckaert, G. Ciccotti, H.J.C. Berendsen, Numerical integration of the cartesian equations of motion of a system with constraints: molecular dynamics of n-alkanes, J. Comput. Phys. 23 (1977) 327–341.
[48] R. Brasseur, Differentiation of lipid-associating helices by use of three-dimensional molecular hydrophobicity potential calculations, J. Biol. Chem. 266 (1991) 16120–16127.
[49] A. Thomas, O. Bouffioux, D. Geeurickx, R. Brasseur, Pex, analytical tools for PDB files. I. GF-Pex: basic file to describe a protein, Proteins 43 (2001) 28–36.
[50] L. Lins, A. Thomas, R. Brasseur, Analysis of accessible surface of residues in proteins, Protein Sci. 12 (2003) 1406–1417.
[51] A. Shrake, J.A. Rupley, Environment and exposure to solvent of protein atoms. Lysozyme and insulin, J. Mol. Biol. 79 (1973) 351–371.
[52] D. Lejeune, N. Delsaux, B. Charloteaux, A. Thomas, R. Brasseur, Protein–nucleic acid recognition: statistical analysis of atomic interactions and influence of DNA structure, Proteins 61 (2005) 258–271.
[53] A. Thomas, B. Joris, R. Brasseur, Standardized evaluation of protein stability, Biochim. Biophys. Acta 1804 (2010) 1265–1271.
[54] E. Eiriksdottir, K. Konate, U. Langel, G. Divita, S. Deshayes, Secondary structure of cell-penetrating peptides controls membrane interaction and insertion, Biochim. Biophys. Acta 1798 (2010) 1119–1128.
[55] L. Kurzawa, M. Pellerano, M.C. Morris, PEP and CADY-mediated delivery of fluorescent peptides and proteins into living cells, Biochim. Biophys. Acta 1798 (2010) 2274–2285.
[56] K. Ezzat, S. El Andaloussi, E.M. Zaghloul, T. Lehto, S. Lindberg, P.M.D. Moreno, J.R. Viola, T. Magdy, R. Abdo, P. Guterstam, R. Sillard, S.M. Hammond, M.J.A. Wood, A.A. Arzumanov, M.J. Gait, C.I.E. Smith, M. HÃ¤llbrink, Ã. Langel, PepFect 14, a novel cell-penetrating peptide for oligonucleotide delivery in solution and as solid formulation, Nucleic Acids Res. 39 (2011) 5284–5298.
[57] H.L. Åmand, B. Nordén, K. Fant, Functionalization with C-terminal cysteine enhances transfection efficiency of cell-penetrating peptides through dimer formation, Biochem Biophys Res Commun. 418 (2012).
[58] W.L. Zhu, S.Y. Shin, Effects of dimerization of the cell-penetrating peptide Tat analog on antimicrobial activity and mechanism of bactericidal action, J. Pept. Sci. 15 (2009) 345–352.
[59] T. Lazaridis, Binding affinity and specificity from computational studies, Curr. Org. Chem. 6 (2002) 1319–1332.